4
Layer-by-layer Coating of Co/Ni Inks for OER

(Cited work: Urgunde et al., Energy Technol. 2019, 7, 9, 1900603)

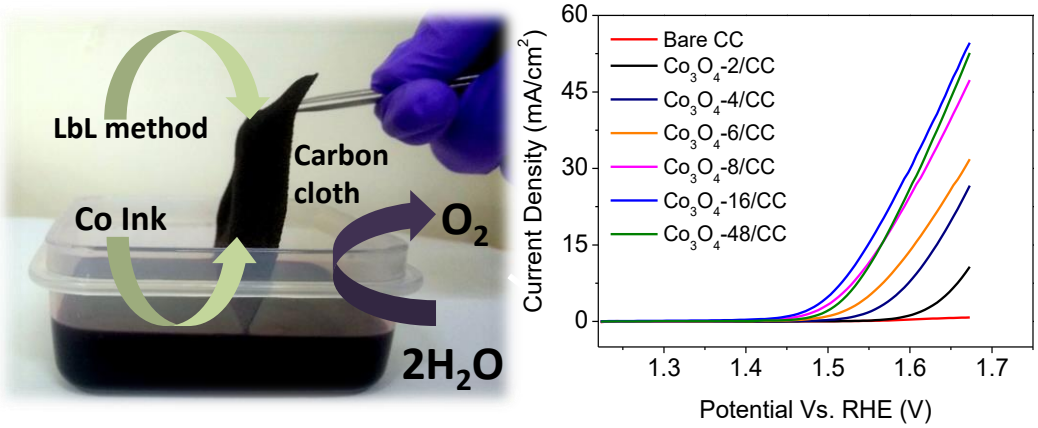

4.1 Introduction

The biggest challenge with electrolysis of water is to reduce the extra overpotential required for water splitting. This can be achieved by tuning the properties of the catalyst. Due to the advantages of the wide availability of water resources, the high purity of hydrogen, and the feasibility of large-scale production, electrochemical water splitting provides a promising method to produce hydrogen via oxygen evolution reaction (OER).[Busupalli et al., 2016; Hisatomi et al., 2014; Mondschein et al., 2017; Tee et al., 2017] IrO_2 and RuO_2 catalysts are known to deliver excellent catalytic performance in OER.[Babar et al., 2018; Subbaraman et al., 2012; Zhu et al., 2017c] The global rareness and high cost of these electrocatalysts hinder their large-scale application. Therefore, it is highly desired to develop highly efficient, affordable, and earth-abundant catalysts that can catalyze OER.[Yan et al., 2015]

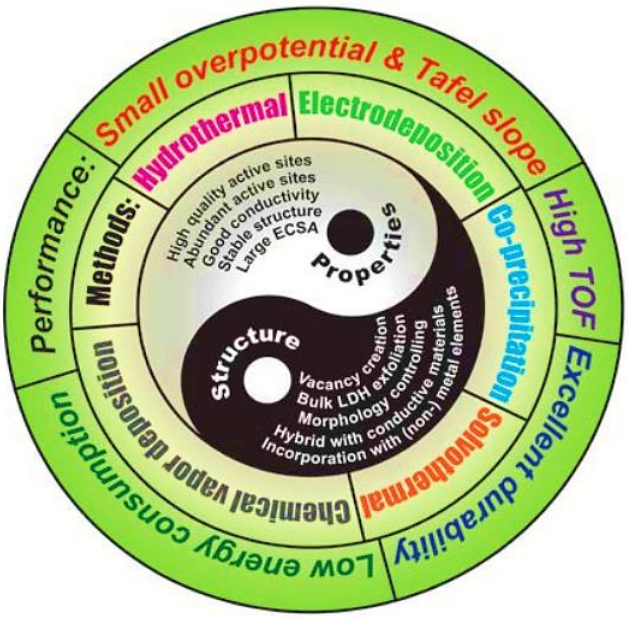

Figure 4.1: Figure of merit, typical synthetic methods and development strategies involved in oxygen evolution reaction. Figure is adapted from [Cai et al., 2019].

The electrocatalytic activity, such as overpotential and stability, still needs improvement to reach the performance of the rare-earth metal electrocatalysts. There are various factors that affect electro-catalytic water splitting such as particle size, catalyst loading, crystallinity, pH of the electrolyte, operating temperature surface morphology and preparative material conditions. The stability of catalyst is a serious concern due to the high resistance of oxide leading to interfacial polarization and poor contact with the current collecting electrode causing leaching of catalytic material in the electrolyte. [Anantharaj et al., 2018] The use of polymeric binders and conductive additives are not so preferred as these lower the OER activity due to poor electrical conductivity.[Zhao et al., 2014] Figure 4.1 shows the graph for figure of merit. It is clear from the plot that a electrocatalyst can be said excellent when the overpotential value lies in the range of 300-400 mV before and after the stability test for 10 h.Hence stability is one of the essential figure of merit while considering OER performance.

The dip and drop coating of a catalytic ink is easy and desirable method however, these are known to perform moderately due to limited loading and surface active sites availability. Herein, we have optimized the catalyst loading by repeated layer-by-layer dip coating of catalyst ink on conducting carbon cloth and compared with direct loading of the catalyst by dip coating in solutions of high concentration followed by thermolysis in both cases. The layer-by-layer method has an advantage of building up the thickness of the catalyst without peeling-off the layer thus increasing the stability of the electrode under operating conditions. The active site and surface area can be further increased by using a light-weight, 3D conducting support system for coating of the catalyst by solution processing. In this study, we have fabricated Co_3O_4 supported on 3D carbon cloth electrodes (Co_3O_4/CC) by repetitive dip coating solution of constant concentration to achieve higher loading and best performance towards OER.

4.2 Objectives of the Work

The objectives of this work are as follows:

1. To develop layer-by-layer deposition method for preparation of Ni and Co oxide on carbon cloth using functional inks.
2. To optimize the deposition parameters (number of dipping and concentration) for best OER performance.
3. To study the electrochemical performance of fabricated electrodes towards OER for practical application.

4.3 Experimental

4.3.1 Synthesis of the Co Hexadecanethiolate and Ni butanethiolate Precursors

The Co-HDT and Ni-BT precursors were synthesized using a general two-step process, detailed in Chapter 2, section 2.4.2.

4.3.2 Characterization of Cobalt Oxide and Nickel Oxide Thin Films

X-ray diffraction pattern was recorded in the 2θ range of 20° to 70° at a scan rate of 0.05°/s using Bruker D8 Advance with Cu Kα (λ=1.5406 Å). The absorbance spectrum was recorded using UV−vis spectrophotometer (Varian Cary 4000) over a wavelength range of 200−800 nm. IR spectrum of Co-HDT was recorded using Fourier transform infrared (FTIR) spectroscopy (Bruker Vertex 70V+PMA5 spectrometer) in the range of 300−4000 cm^{-1}. Morphological changes were examined by field–emission scanning electron microscopy (Nova NanoSEM 600 instrument, FEI Co., The Netherlands) equipped with EDS detector. TEM imaging was performed by transmission electron microscope (FEI Tecnai-G2 T20). For imaging, ~10 mg of

the sample was dispersed in ethanol and drop coated on a copper grid and allowed to dry before imaging. Raman Spectrum was recorded using a confocal Raman microscope (Renishaw, UK) with a semiconductor diode laser with excitation source (0.5% power) at an emission wavelength of 523 nm. X-ray photoelectron spectrum (XPS) analysis was conducted with Thermo scientific NEXSA surface analysis X-ray photoelectron spectroscope equipped with Al Kα radiation, and the binding energy was calibrated by the C 1s peak (284.6 eV) of contamination carbon. The active mass estimation was done using CHNS analysis and TGA analysis. CHNS analysis of Ni-BT and Co-HDT complex for molecular formula and weight estimation was performed using Elementary Vario EL-III equipment. Thermogravimetric analysis of Co-HDT complex (10 mg) was performed at a rate of 10 °C/min in N_2 atmosphere by using Simultaneous Thermal Analyzer, Perkin Elmer equipped with a digital temperature controller from Poly Science (Table 4.1).

Table 4.1: CHNS analysis of $Co(SC_{16}H_{33})_2$ for active mass estimation.

Compound	C % by (theoretical)	C% by (CHNS)	H% (theoretical)	H% by (CHNS)	S% (theoretical)	S% by (CHNS)
Co-HDT	70	60.57	11.57	11.60	11.80	9.12
Ni-BT	60.75	70	11.57	12	9.12	11.80

4.3.3 Electrochemical Characterization

All electrochemical properties were studied on CHI660E electrochemical workstation in a three-electrode configuration containing an Ag/AgCl reference electrode and Pt as a counter electrode. All the measurements were performed in 1 M aqueous KOH electrolyte solution at pH 14. The pH of the electrolyte was varied by changing the concentration of KOH electrolyte wherever specified. Catalyst loaded on carbon cloth was used as working electrode. The potential of the working electrode was linear with a constant scan rate in a specific range. All potentials were calculated with respect to a reversible hydrogen electrode (RHE). Linear sweep voltammetry (LSV) was recorded at 1 mV/s. From LSV, oxygen evolution reaction (OER) activities of the catalysts were evaluated by the overpotential (Ƞ) required for the current density of 10 mA/cm^2 (current density is a typical value to match a 10% efficient solar water-splitting device under 1 sun illumination). Polarization curves were obtained from LSV measurements at 1 mV/s and Tafel slope, *b* is calculated by using the equation given in section The Co Hexadecanethiolate and Ni butanethiolate Precursors was synthesized using general two step process which is detailed in section 2.6 of chapter 2. The stability of the electrocatalyst was investigated by conducting the chronopotentiometry (CP) of the catalyst at a constant current density of 10 mA/cm^2. All polarization curves and chronopotentiometry curves are shown without any iR compensation. The results are presented without iR compensation to understand the actual contribution of the overpotential from the active material since the total resistance of the system can get influenced by the overpotential values.[Anantharaj et al., 2018]

4.4 Results and Discussion

4.4.1 Characterization of Co Hexadecanethiolate (Co-HDT)

Co-HDT-based ink is synthesized following a modified method reported for Ni alkanethiolates in the literature.[Gupta et al., 2017a; John et al., 2007b; Urgunde et al., 2018] Briefly, cobalt triethylamine complex is mixed with hexadecane thiol in 2:1 molar ratio to form Co-HDT complex. The compound was obtained as precipitate and further dissolved in toluene to make a clear solution and characterized by UV-visible and FTIR spectroscopy (Figure 4.2a and b). The

thermogravimetric analysis in Figure 4.3a shows that the decomposition of Co-HDT ink occurs at 320 °C with no further weight loss indicating complete removal of organics. Thus, a thermolysis temperature of 350 °C in N_2 atmosphere was chosen for the preparation of Co_3O_4 electrocatalyst.

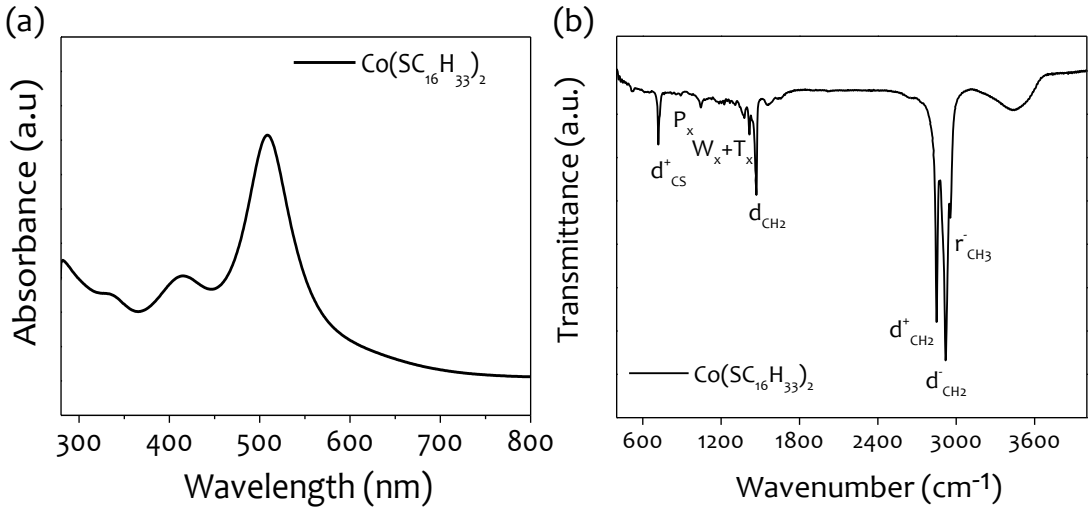

Figure 4.2: (a) UV-visible spectrum and (b) FT-IR spectrum of Co-HDT complex in solution.

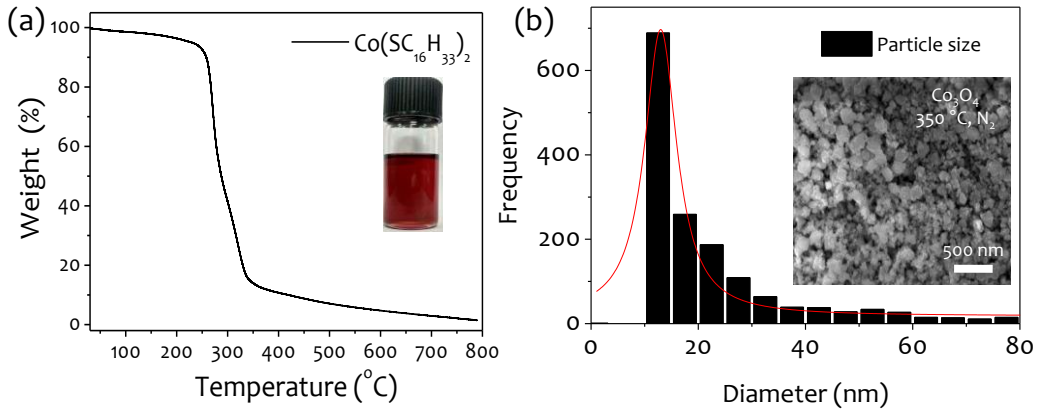

Figure 4.3: (a) Thermogravimetric analysis (TGA) of Co-HDT precursor at 10 °C/min in N_2 atmosphere. (b) Particle size distribution of Co_3O_4 from FESEM image (inset) analysis in Image J software as seen in the insets.

SEM image in insets of Figure 4.3b clearly shows the formation of small yet irregular-shaped crystalline nanoparticles. The average particle size of Co_3O_4 nanoparticles was calculated to be ~ 15 ± 3.8 nm (Figure 4.3b). As revealed by the XRD pattern in Figure 4.4a, the decomposition of Co-HDT ink resulted in the formation of pure cobalt oxide (Co_3O_4) with typical cubic spinel structure (JCPDS file number 78-1970).The Raman spectra in Figure 4.4b exhibit peaks at 191, 467, 487, 608, and 672 cm^{-1} that clearly correspond to spinel-Co_3O_4. The peaks at 467 and 608 cm^{-1} correspond to E_g and F_{2g} respectively and are related to the combined vibrations of octahedral oxygen motion and tetrahedral sites while the Raman mode at 672 cm^{-1} is attributed to the characteristics of the octahedral site, A_{1g}.[Hadjiev et al., 1988; Yeo et al., 2011a]. The TEM image of the Co_3O_4 powder obtained by scratching it off from the substrate is shown in Figure 4.4c. The nanoparticles with different lattice spacing could be seen clearly in HRTEM image (Figure 4.4c). An interplaner spacing of 0.46 nm and 0.24 nm corresponds to (111) and (311) planes of cubic Co_3O_4 respectively (Figure 4.4d). The formation of Co_3O_4 is further confirmed from SAED pattern (Figure 4.4e) with the concentric rings assigned to the lattice planes (111), (220), (311) and (222). The weak yet bright diffraction spots indicate the polycrystalline nature of Co_3O_4.

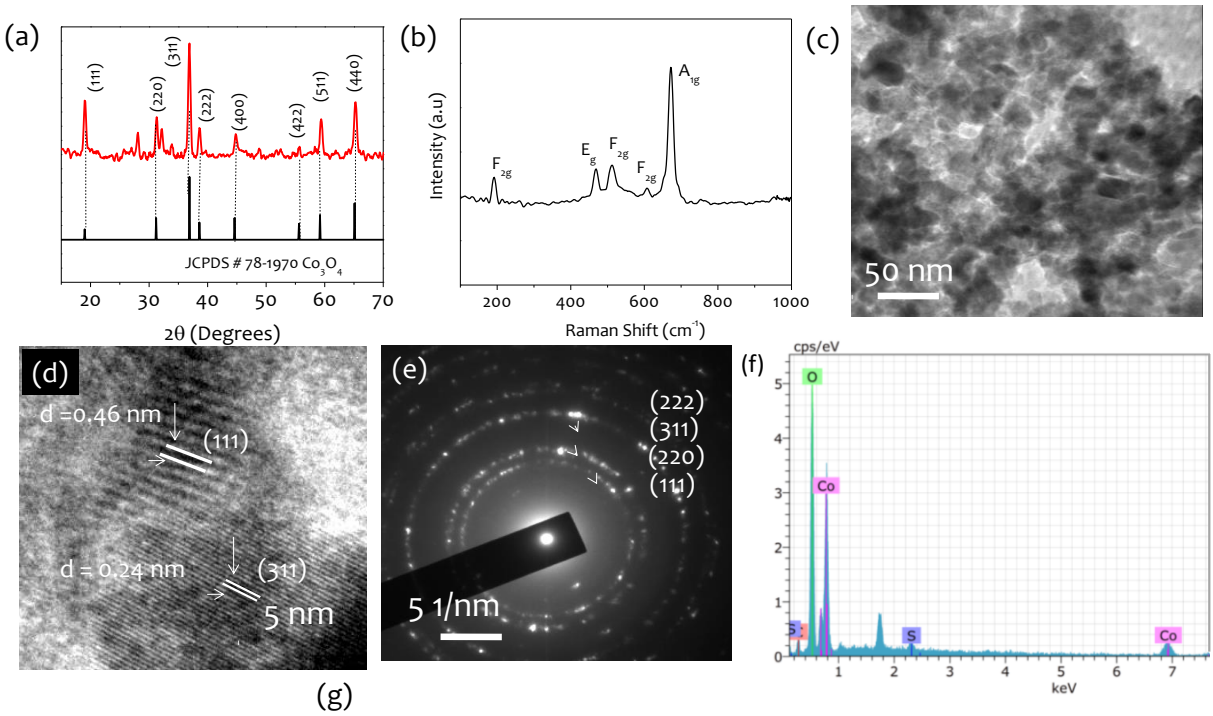

Figure 4.4: (a) X-ray diffraction pattern, (b) Raman spectrum, (c) Transmission Electron Microscopy (TEM) image, (d) High Resolution Transmission Electron Microscopy (HRTEM) image and (e) Selected Area Electron Diffraction (SAED) pattern of Co_3O_4 films prepared by thermolysis of Co-HDT at 350 °C in N_2 atmosphere. (f) Energy Dispersive Spectroscopy (EDS) analysis of Co_3O_4.

Energy dispersive X-ray spectroscopy (EDX) was carried out to study the composition of elements present in the compound to vindicate the patterns observed in XRD. Figure 4.4f shows an additional presence of sulfur and carbon along with signals from cobalt and oxygen. The stoichiometric defects could be present due to the presence of carbon and sulfur residues in the lattice.

4.4.2 Fabrication of Co_3O_4/CC Electrodes by LbL coating of Co-HDT

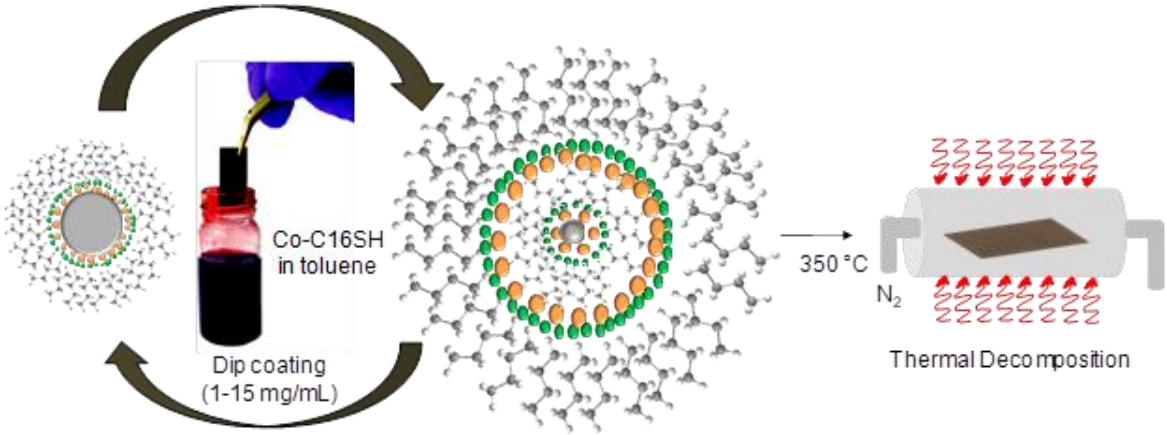

Figure 4.5: (a) Schematic demonstrating the dip coating method adopted for the fabrication of functional electrode materials based on a Co_3O_4/CC system for OER.

The Co-HDT ink is coated on carbon cloth by LbL assembly method as shown schematically in Figure 4.5. In this approach, the carbon cloth electrode is dipped repeatedly in the Co-HDT ink of moderate concentration (5 mg/mL) and air dried to build up the electrode thickness followed by thermolysis at 350 °C in N_2. To avoid any effect of the subsequent dipping on the previous coating, the dipping time was kept much lower than that required for dissolution of the dried

coating. LbL assembly is advantageous as it not only allows higher loading of material despite of limited solubility of precursor but also result in stability of material in terms of adhesion to carbon cloth surface during electrochemical testing. As a control, solutions of different concentrations (1, 5, 10 and 15 mg/mL) are directly coated on the carbon cloth and thermolysed at 350 ^{o}C in nitrogen resulting in the formation of the electrocatalytic layer of Co_3O_4 on carbon cloth. However, since the solubility of these complexes is limited, concentration beyond 15 mg/mL in toluene for higher loading could not be obtained.

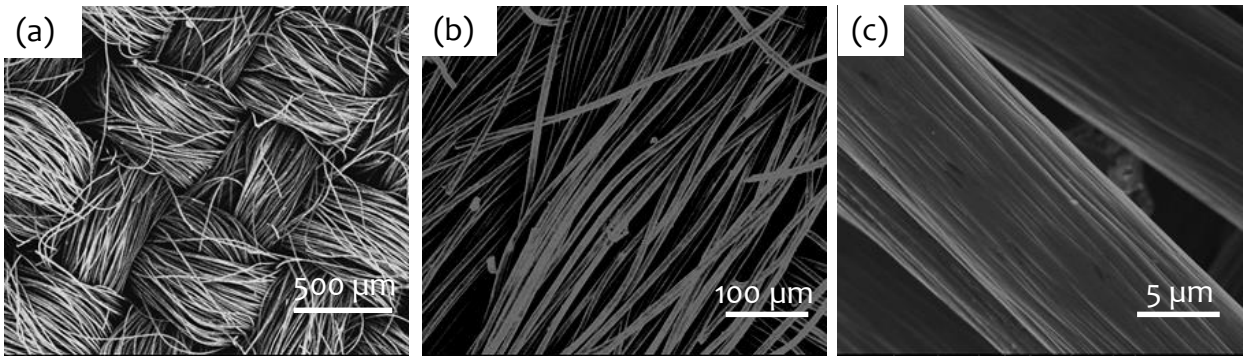

Figure 4.6: FESEM images of (a-c) pristine carbon cloth.

The pristine carbon cloth surface before coating of Co_3O_4 is shown in Figure 4.6. The bird-eye view of Co_3O_4/CC electrode is shown in Figure 4.7. The FESEM image in Figure 4.7b and c shows the magnified view of surface coverage of carbon fibre by Co_3O_4 nanoparticles. Most regions on carbon fibre are coated with Co_3O_4 material except a few areas as seen in Figure 4.7d.

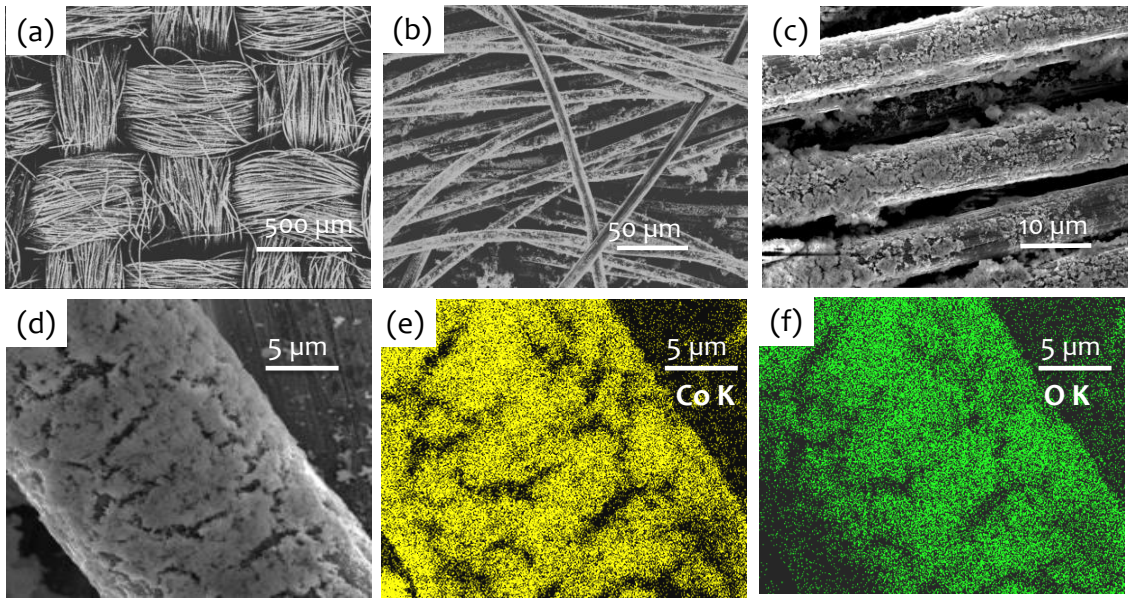

Figure 4.7: (a-c) FESEM images of Co_3O_4/CC electrodes at different magnifications. (d-f) EDS mapping of Co Kα, and O Kα from carbon fibre coated with Co_3O_4.

The EDS mapping of Co_3O_4/CC electrode in Figure 4.7e and f shows uniform distribution of Co and O respectively across the fibre surface. The surface modifications in Co_3O_4/CC leading to the increase in electrochemical activity are mechanistically studied by XPS measurements before and after 50 cycles of electrooxidation in alkaline medium. The survey spectrum of the catalyst indicated the presence of S along with Co, O and C (Figure 4.8a). However, the absence of peak at 162.5 eV in high-resolution spectrum indicates the absence of Co-S bond. In the S 2p spectrum (Figure 4.8b), the peak is deconvoluted into three peaks at 166.4, 168.3 and 169.4 eV and are associated with –C-SO_x-C (x = 2,3,4) species respectively and are considered

electrochemically inactive. The increase in carbon concentration after electrochemical testing of 50 cycles is attributed to the adsorption of CO_2 from the atmosphere (Figure 4.8c).

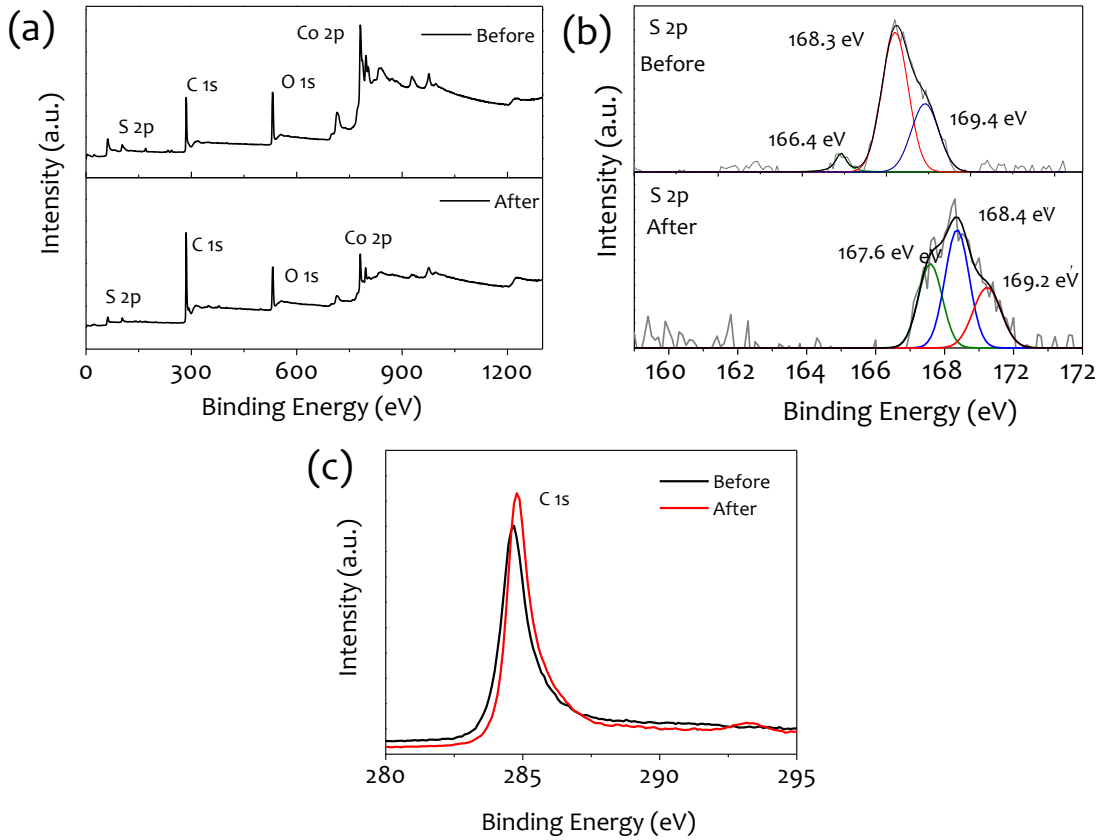

Figure 4.8: (a) Full survey spectra, high-resolution spectra of (b) S 2p and (c) C 1s before and after electrochemical oxidation for 50 test cycles.

Since the intensity decreases considerably on oxidation, it is clear that sulphur present in the compound does not play any important role in water oxidation. Figure 4.9a represents high-resolution Co 2p spectrum for the as-prepared electrode which consists of two main broad peaks corresponding to $2p_{1/2}$ and $2p_{3/2}$ spin-orbit coupling along with two shakeup satellite peaks at 785.7 eV and 802.5 eV. The binding energies (BEs) of Co $2p_{3/2}$ and $2p_{1/2}$ are separated by 15 eV indicating presence of Co^{3+} species on the surface. However, the ratios of Co^{2+}/Co^{3+} in the case of as prepared electrode is 1.5 which is three times higher than that expected for spinel Co_3O_4 indicating additional presence of $Co(OH)_2$ species. During OER, due to oxidation of Co^{2+} to Co^{3+}, there is a change in the satellite structure as well as the increase in Co^{2+}/Co^{3+} to 1.57 due to the transformation of $Co(OH)_2$ to the active CoOOH phase as seen in Figure 4.9b. After electrochemical testing of 50 cycles, Co^{2+} in $Co(OH)_2$ is characterized by the Co $2p_{3/2}$ peak at 780.8 eV and its satellite at a distance of 5.0 eV which corresponds to the CoOOH formation. This is confirmed by the shift of the Co $2p_{3/2}$ peak to a binding energy of 780.3 eV and the appearance of the Co^{3+} satellite at a distance of 10 eV after the electrochemical test. Thus, the oxidation of water in presence of alkaline medium mainly involves Co_3O_4 conversion to CoOOH. The O1s spectrum shown in Figure 4.9c after OER shows a sharp peak at 529.2 eV which is associated with oxygen in metal oxide and at 530.7 eV due to hydroxide and per-hydroxide species. The O 1 s spectrum of the as prepared electrode exhibits the peaks at 530.8 eV which is associated with hydroxide group (OH^-) and three more peaks at 529.3, 531.5, and 532.3 eV correspond to Co-O, oxygen vacancies and structural water (Figure 4.9d). The oxygen vacancies lower the adsorption energy for water and increase the conductivity of Co_3O_4 leading to an enhanced OER activity.

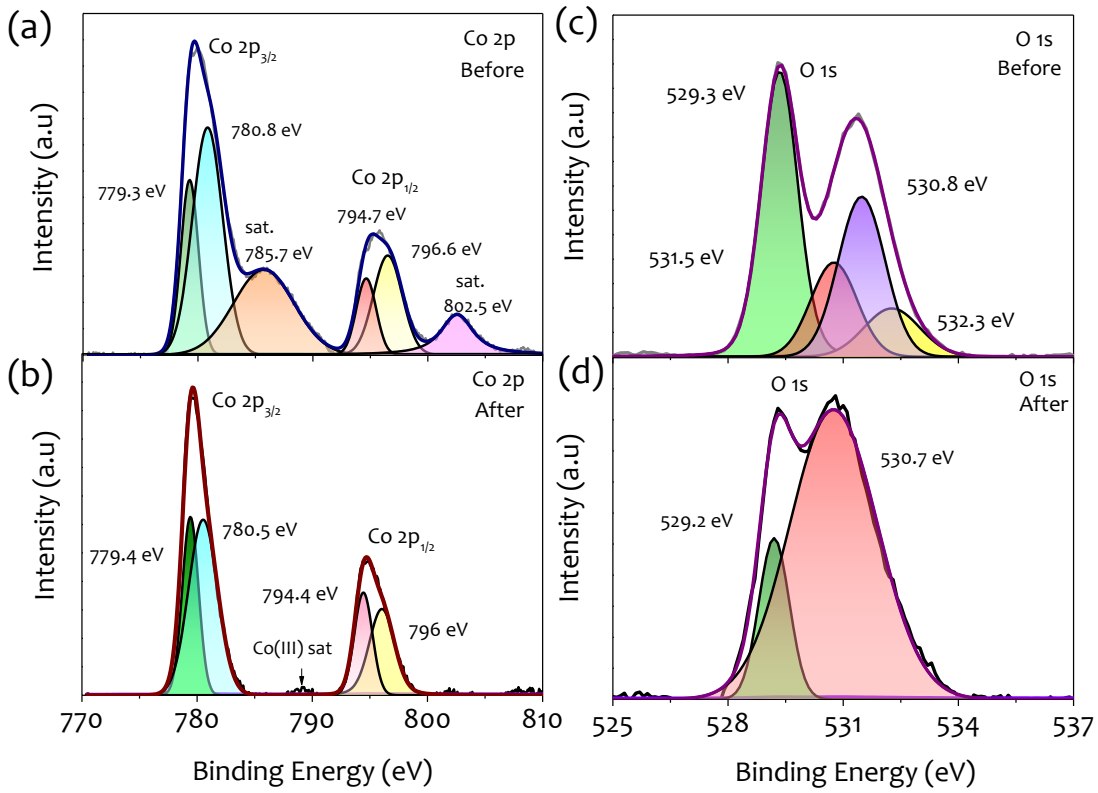

Figure 4.9: High resolution XPS spectra of (a,b) Co 2p and (c,d) O1s of Co_3O_4/CC before and after electrochemical testing (50 cycles) respectively.

4.4.3 Electrochemical Performance of Co_3O_4/CC Electrodes

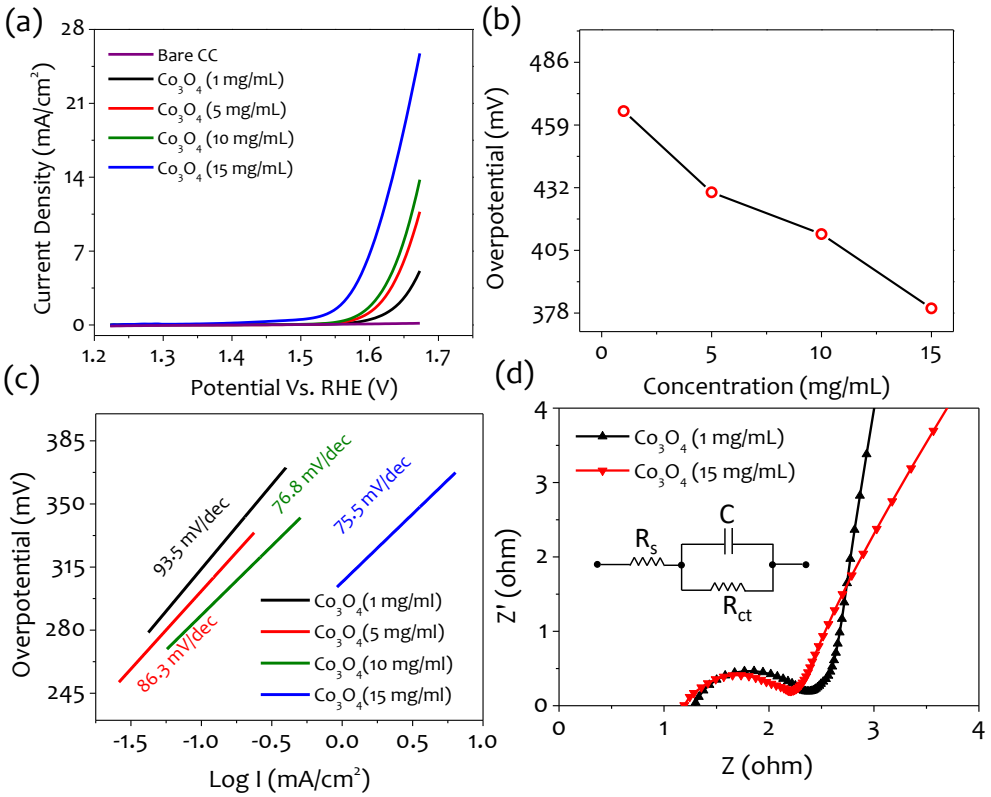

Figure 4.10: OER activity from Co_3O_4/CC electrodes fabricated by single time dip coating in precursor of different concentrations of Co-HDT ink and annealing at 350 °C in N_2. (a) LSV curves and the variations in (b) Overpotential values corresponding to concentration of the solution (c) Tafel slope analysis and (d) EIS analysis.

For water splitting activity, Co_3O_4/CC was studied by electrochemical OER in 1 M KOH as an electrolyte in three-electrode geometry. The Co_3O_4 electrodes were prepared by directly dip coating of the precursor of different concentrations (1, 5, 10 and 15 mg/mL) followed by annealing. As seen from the linear sweep voltammetry (LSV) curves (Figure 4.10a), the anodic current from Co_3O_4/CC electrode increases with higher loading of Co_3O_4 on CC as expected. It can be clearly observed that the Co_3O_4 with higher mass loading of 15 mg/mL exhibit much higher OER activity with high current density. The OER onset potential decreases with increasing loading of the catalyst as shown in Figure 4.10b. The best OER onset overpotential required for driving current density of 10 mA/cm² in Co_3O_4 is ~380 mV. The Tafel slope is obtained by re-plotting the low overpotential region of the LSV curves (Figure 4.10c). The lowest value of the Tafel slope for Co_3O_4/CC (prepared using 15 mg/mL) is 75.5 mV/dec. It clearly suggests better OER catalytic kinetics compared to many other literature reports tabulated in Table 1.5. From the EIS analysis in the Nyquist plot (Figure 4.10d), it can be seen that the higher loading gives better charge transfer of an electron through the interface between electrode and electrolyte. The charge transfer resistance, R_{CT} value which is the connotation for the kinetics of a reaction, is lowered from 447.4 Ω to 210.1 Ω with an increase in loading from 1 mg/ml to 15 mg/mL indicating a higher kinetic rate of the OER.

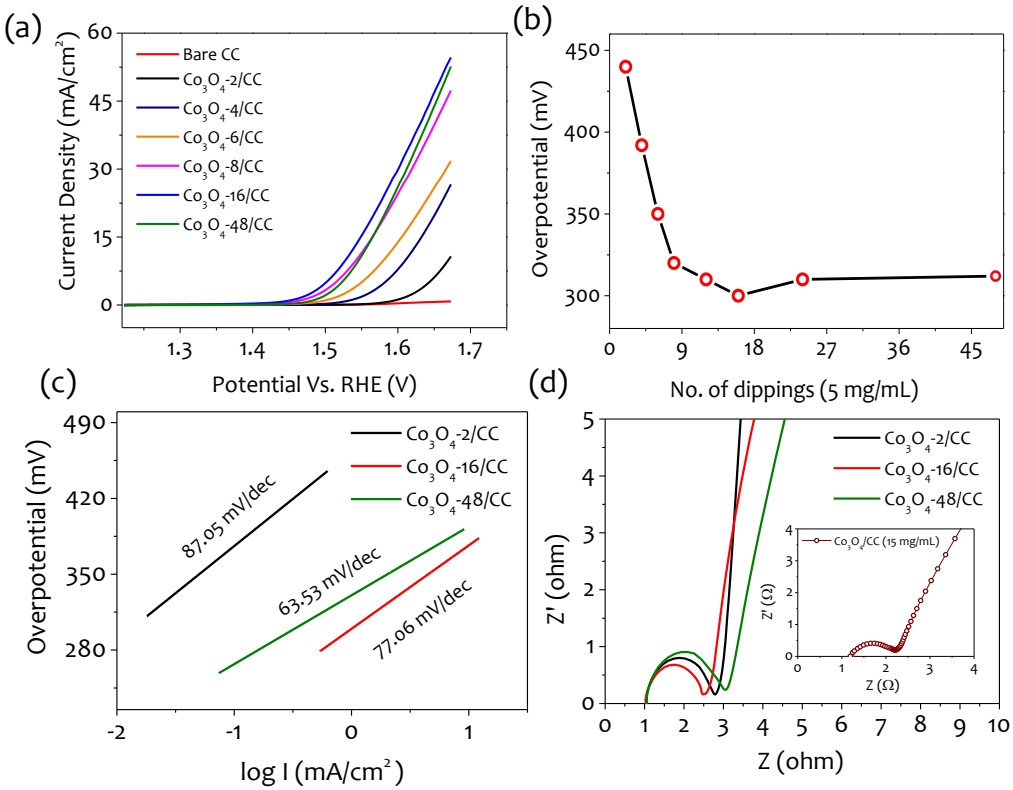

Figure 4.11: OER activity of Co_3O_4/CC electrodes fabricated by LbL assembly of Co-HDT and thermolysis at 350 °C in N_2. (a) LSV curves, (b) variations in overpotential values corresponding to dipping number in solution (c) Tafel slope analysis, (d) Nyquist plots.

LSV curves of the Co_3O_4/CC electrode with different loading of the catalyst prepared by varying the dipping number in a precursor solution of 5 mg/mL are shown in Figure 4.11a. The OER activity could be improved by optimizing the catalyst loading amount by repeated dip coating of the precursor. Remarkably, there is a systematic increase in current densities with an increase in dipping number. In Co_3O_4-16/CC (index 16 refers to 16 times dipping), the overpotential at 10 mA/cm² was observed to be lowest (300 mV) without any iR compensation. Beyond the threshold number of dips, the overpotential remained constant with no further mass dependent OER activity (Figure 4.11b). However, the exact loading in terms of mass is difficult to determine precisely since there is a mass loss of the substrate during annealing.

The Tafel slopes were examined from LSV curves measured at 1 mV/s to understand the kinetics of the OER. In the case of spinel Co_3O_4-48/CC (Figure 4.11c), the Tafel slope is 63.5 mV/dec lowest indicating faster OER kinetics. In comparison to many cobalt-based OER systems, the value obtained from pristine Co_3O_4 is quite appreciable. The EIS analysis in Figure 4.11d shows that the R_{CT} value for dip coated samples for Co_3O_4–16/CC is further reduced to 53.7 Ω while it increases for Co_3O_4–48/CC to 131.8 Ω for an increased number of dipping. Thus, Co_3O_4 seems to possess optimum characteristics for a better catalyst.

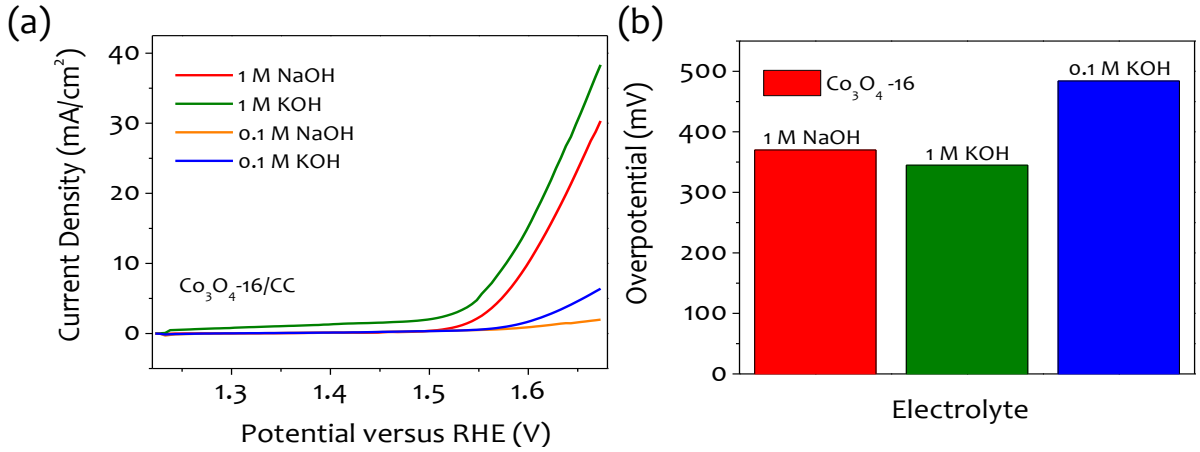

Figure 4.12: (a) LSV curves of Co_3O_4-16/CC in 1 M and 0.1 M of KOH and NaOH. (b) Bar graphs representing the effect of concentration and alkaline medium on overpotential for Co_3O_4 -16/CC electrode.

The influence of alkaline medium and concentration on OER was studied by LSV measurements (Figure 4.12a and b). The absence of oxidation peaks indicates that the overall reaction kinetics is controlled by the number of active sites. In the case of 1 M NaOH, the current decreased drastically as compared to that of 1 M KOH. Clearly, the OH^- concentration in the electrolyte is important for the overall catalytic performance and enhanced kinetics. The turnover frequency (TOF) is defined, as the number of moles of O_2 evolved per unit time at single active site. It is an important index for the evaluation of the intrinsic OER activity of the electrocatalyst. From the measurements, the TOF of Co_3O_4–16/CC is 0.13 s^{-1} at the overpotential of 300 mV, which is higher than that of Co_3O_4–2/CC (0.0022 s^{-1}) and Co_3O_4–48/CC (5.60 × 10^{-3} s^{-1}).

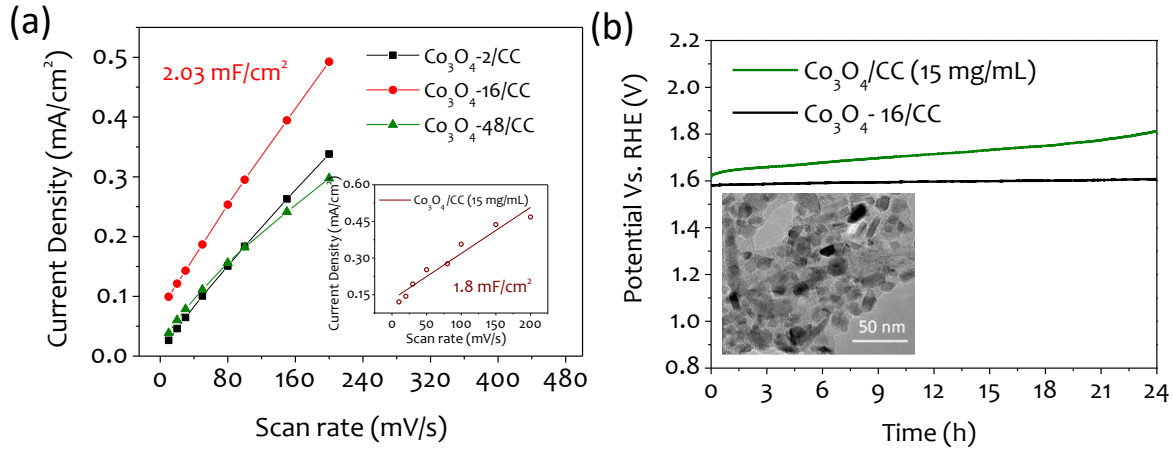

Figure 4.13: (a) Double-layer capacitance calculation and (b) Chronopotentiometry of Co_3O_4/CC electrodes for different loading density by dip coating compared with electrodes prepared by multiple dip coating with a constant loading density and Inset shows the HRTEM image of Co_3O_4 particles embedded in the carbon matrix. Note that the running number in all legends corresponds to the dipping number.

The electrochemically accessible surface area (ECSA) and electric double-layer capacitance (C_{dl}) can help in understanding the trend in the activity of different catalytic systems. Since C_{dl} is directly related to the ECSA, the value of C_{dl} for Co_3O_4-16/CC (2.03 mF/cm²) and that obtained

by directly dip coating of 15 mg/mL (1.8 mF/cm²) catalyst is comparable and relatively higher than Co_3O_4-2/CC and Co_3O_4-48/CC samples (Figure 4.13a and Figure 4.14).
Clearly, the Co_3O_4 prepared by repeated dip coating displays equivalent intrinsic catalytic activity as that by conventional dip-coating in high concentration solution (15 mg/mL) without compromising the surface reactivity. Chronopotentiometry (CP) of Co_3O_4 prepared by direct dip-coating as well as repeated dip coating was conducted to check the stability and durability of the catalyst**.** As seen in the Figure 4.13b, the chronopotentiometric response for Co_3O_4-16/CC was found to be very stable with insignificant changes in the overpotential with respect to time as compared to Co_3O_4 prepared by direct loading (dip coating in 15 mg/mL) in which the potential increased steadily to 1.8 V within 24 h clearly demonstrating the instability of these electrodes. The decomposition of the carbon chain of the thiolates results into formation of a carbon matrix supporting the catalyst particles. This carbon matrix formed acts as an adhesion medium between the catalyst nanoparticles and the CC resulting into a better adhesion.The increase in overpotential could be due to the non-uniform deposition in single time dipping, agglomeration of particles during annealing, and instability at electrode-electrolyte interface resulting in leaching of the catalyst from the carbon cloth surface in case of the directly loaded Co_3O_4 sample by single time dip coating. Clearly, in case of Co_3O_4-16/CC with repeated dip coatings, a continuous layered structure is formed that on annealing lead to robust yet highly active Co-O catalytic sites with better adhesion to the substrate in contrast to that of a conventional dip-coating method.

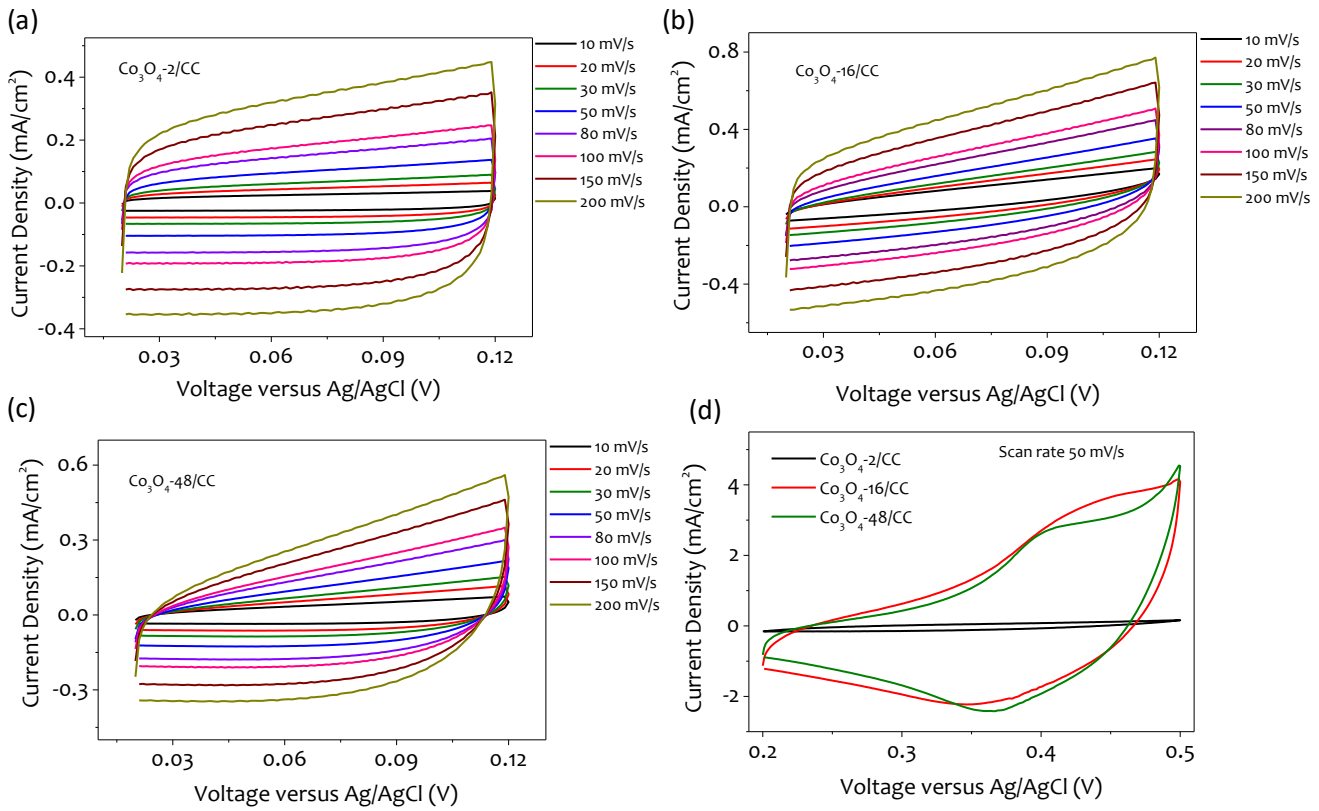

Figure 4.14: Cyclic Voltammetry (CV) curves of (a) Co_3O_4-2/CC, (b) Co_3O_4-16/CC, and (c) Co_3O_4-48/CC at different scan rates in faradic region (d) Comparative CV curves of Co_3O_4-2/CC, Co_3O_4-16/CC, and Co_3O_4-48/CC in non-faradic range for relative specific capacitance.

4.4.4 Material Characterization and Fabrication of NiO/CC Electrodes

The TGA of Ni butanethiolate was carried out to check the decomposition temperature (Figure 4.15a). A stable weight% profile was observed after 250 °C; hence the 350 °C was chosen to optimum temperature to obtain NiO as electrocatalyst by annealing Ni-BT. XRD was carried out to understand the phases present in the formed electrocatalyst (Figure 4.15b). XRD pattern

confirms the formation of pure NiO with FCC structure (JCPDS file number 47-1049) after the decomposition of Ni-BT ink (Figure 4.15b). The highest peak intensity is observed for 200 planes. For the application as an electrocatalyst, the Ni-BT ink was coated on carbon cloth by LbL assembly technique as previously done in the case of Co-HDT and annealed in nitrogen at 350 °C.

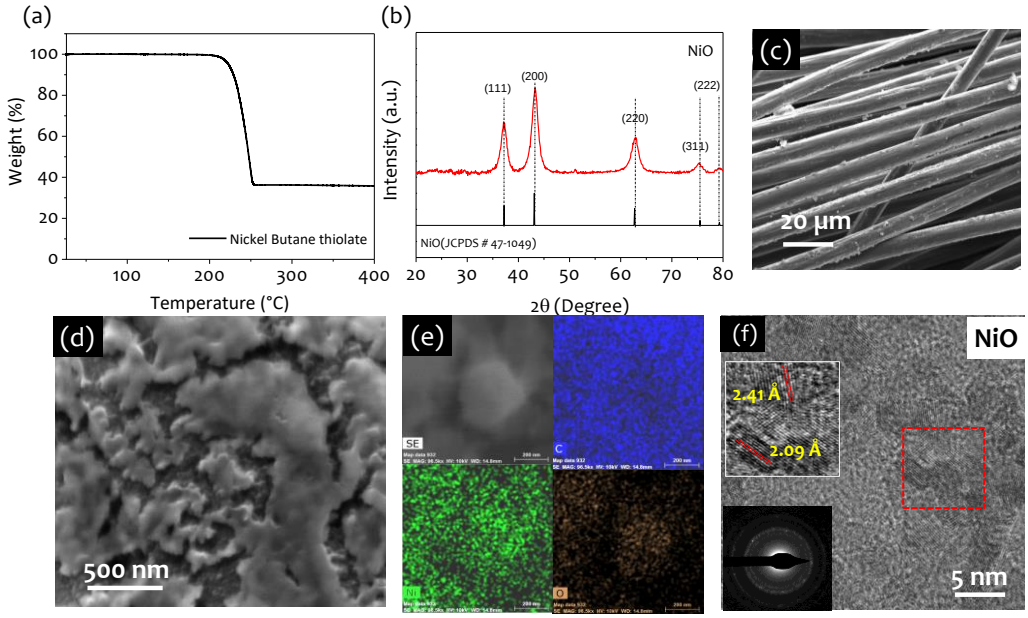

Figure 4.15: (a) Thermo gravimetric analysis of Ni-BT. (b) X-ray diffraction pattern, (c-d) FESEM, (e) elemental mapping, and (f) HRTEM (Insets with magnified image and SAED pattern) on carbon cloth obtained after annealing Ni-BT in N2 at 350 °C.

The bird-eye view of the NiO/CC electrode is shown in Figure 4.15c. The FESEM image shows the uniform coating of NiO on the carbon fiber of the CC. The FESEM image in Figure 4.15d and e shows the NiO nanoparticles formed on the surface with EDS mapping showing the uniform distribution of Ni and O across the surface of the fiber. Figure 4.15f shows the HR TEM image with a zoomed view and SAED pattern. The d spacing was analyzed using GATAN GSM, and interplanar spacing of 0.241 nm corresponds to the 111 plane and 0.209 nm to 200 plane of NiO, respectively. The SAED pattern confirms the presence of polycrystalline nature with diffuse ring accompanied with the spots.

4.4.5 Electrochemical Performance of Ni-BT based Electrodes

In a similar way, Ni-BT was layer by layer coated on carbon with increasing concentrations of 1, 5, 10, and 15 mg/mL. The electrodes formed after annealing were studied in 1 M KOH solution in three-electrode geometry. As seen from the linear sweep voltammetry (LSV) curves (Figure 4.16a), the anodic current of the NiO/CC electrode increases with increasing loading of NiO on CC. It is clearly evident that the NiO with higher mass loading of 15 mg/mL exhibits higher OER activity with high current density. The onset potential also showed an increment with an increase in the loading of the catalyst. A similar trend was found with the overpotential (@10 mA/cm^2). The NiO-15 mg/mL had the lowest overpotential of 400 mV (Figure 4.16b). The Tafel slope was plotted using the LSV curves (Figure 4.17a), the lowest Tafel slope for NiO-15 mg/mL 85.1 mV/dec. From the EIS analysis and the Nyquist plot (Figure 4.17b), it is seen that the highest loading of 15 mg/mL offered lower charge transfer resistance compared to the highest current loading. The improvement in the OER activity as shown for Co_3O_4/CC electrode can be implemented for NiO by optimizing the Ni-BT loading by repetitive dip coating of the precursor. The LSV was carried out for a different number of Ni-BT dip coatings on CC after annealing, as shown in Figure 4.18a.

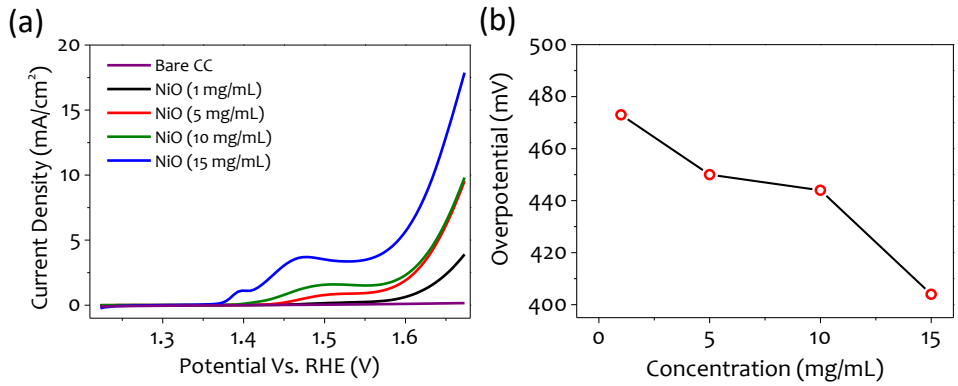

Figure 4.16: OER activity from NiO/CC electrodes fabricated by single time dip coating in precursor of different concentrations of Co-HDT ink and annealing at 350 °C in N_2. (a) LSV curves and the variations in (b) Overpotential values corresponding to concentration of the solution.

There is a significant increase in current density with an increase in the number of dippings. The highest current density was observed for NiO-24/CC, contrary to 16 times dip-coating observed in the case of Co_3O_4 electrodes (Figure 4.18a). The overpotential was calculated at 10 mA/cm^2, and the lowest overpotential was 340 mV of NiO-24/CC without any iR compensation (Figure 4.18b).

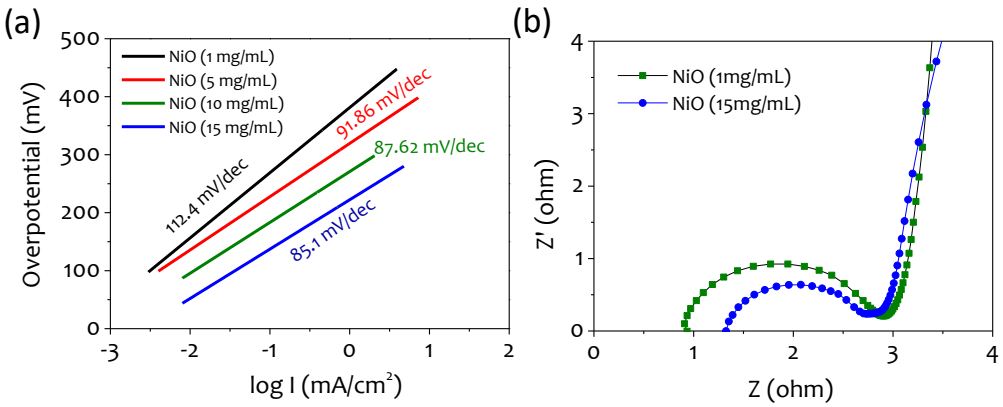

Figure 4.17: (a) Tafel slope analysis and (b) EIS analysis of NiO/CC electrodes fabricated by single time dip coating in precursor of different concentrations of Co-HDT ink and annealing at 350 °C in N_2.

Tafel slopes were calculated from the Tafel plot using LSV (Figure 4.19a). The Tafel slope of 65 mV/dec was the lowest indicating faster OER kinetics with a similar trend in the case of NiO-24/CC. From the measurements, the TOF of NiO–24/CC the overpotential of 340 mV. Clearly, the NiO electrode with different dip-coating displays higher intrinsic chemical activity towards OER compared to dip-coating in high concentration solution (15 mg/mL).

The chronopotentiometry of the electrode was studied by applying a current density of 10 mA/cm^2. As seen in Figure 4.19b., the chronopotentiometric response for NiO-24/CC was found to be stable with insignificant changes within the overpotential compared to NiO-15 (dip-coating in 15 mg/mL) for 24 h, clearly demonstrating the stability of LBL (NiO-24/CC) coated electrode those electrodes.

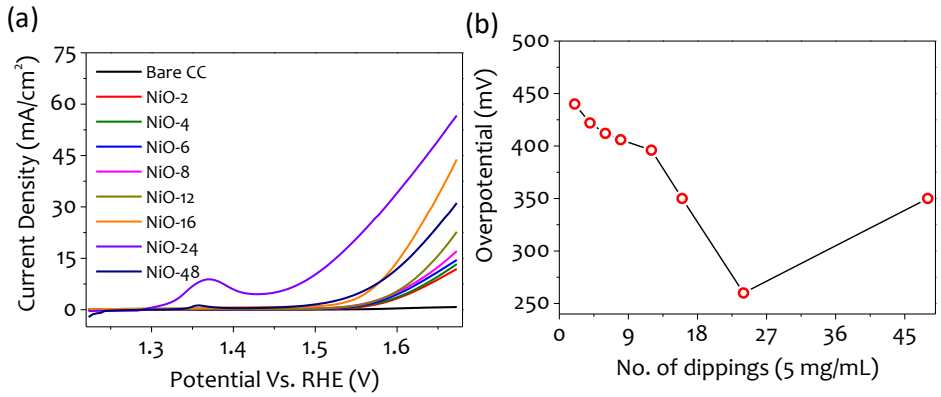

Figure 4.18: OER activity of NiO/CC electrodes fabricated by LbL assembly of Co-HDT and thermolysis at 350 °C in N_2. (a) LSV curves, (b) variations in overpotential values corresponding to dipping number in solution.

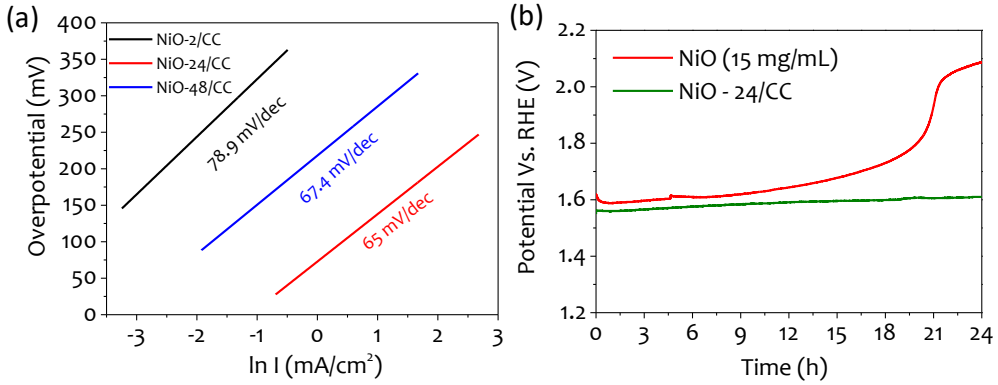

Figure 4.19: (a) Tafel slope analysis, (b) Nyquist plots of NiO/CC electrodes fabricated by LbL assembly of Co-HDT and thermolysis at 350 °C in N_2.

4.5 Conclusions

In conclusion, Co-HDT complex and Ni-BT were synthesized by a simple, solution-based method were used for the fabrication of polycrystalline Co_3O_4 and NiO electrodes conformably coated as a thick layer on conducting carbon fibre cloth as substrate. A repeated LbL dip-coating method is adopted in this study for achieving the optimum loading density of the catalyst on the carbon cloth substrate. The catalyst loading is increased on carbon cloth surface by successive dip coating. With the increasing dip coating number, the onset potential decreases and saturates after 16 and 24 times dip coating of Co hexadecane thiolate and Ni butane thiolate respectively followed by thermal decomposition step. The decrease in onset potential is understandable due to the decrease in charge transfer resistance and increase in ESCA till a uniform surface coverage is achieved by repeated dip coating. As observed, onset potential become constant beyond a certain coating number since there is only an increase in thickness without significant change in the intrinsic resistance and surface area of the electrocatalyst. The surface reactivity and mechanism for OER activity is examined by XPS analysis. The overpotential of Co_3O_4/CC is reduced from 380 mV to 300 mV and Tafel slope of 75.5 mV/dec is lowered to 63.5 mV/dec by LbL method in contrast to conventional dip coating. A similar trend is observed in case of Ni-BT LBL coating the lowest overpotential and Tafel slope of 340 mV and 65 mV/dec was observed in NiO-24/CC sample. The electrocatalytic activity is observed to be mass and surface sensitive and independent of the coating method and offers great potential as an efficient catalyst. This proves that the material is highly efficient for electrochemical water splitting application.